I&EC research
Industrial & Engineering Chemistry Research

pubs.acs.org/IECR

Article

Controlled Hydrolysis of TiO_2 from HCl Digestion Liquors of Ilmenite

Richard G. Haverkamp,* Kia S. Wallwork, Mark R. Waterland, Qinfen Gu, and Justin A. Kimpton

Cite This: *Ind. Eng. Chem. Res.* 2022, 61, 6333−6342

Read Online

ACCESS | Metrics & More | Article Recommendations | Supporting Information

ABSTRACT: Traditionally, industrial scale production of the TiO_2 pigment is achieved by hydrolysis from H_2SO_4 solution or by hydrolysis of $TiCl_4$. However, the H_2SO_4 route produces $FeSO_4$ waste, which is problematic, and the $TiCl_4$ route requires a high grade rutile feedstock or chemically upgraded ilmenite ($FeTiO_3$). Here, we investigate a direct route from ilmenite to TiO_2 using aqueous HCl. New Zealand ilmenite digested in 35 wt % HCl to achieve a solution containing typically 1.18 mol kg^{-1} $Fe_{(aq)}^{2+}$ and 1.14 mol kg^{-1} $Ti_{(aq)}^{4+}$ was hydrolyzed under reflux, after seed preparation in water, or with phosphoric or citric acid. The structure of the seed was determined by Raman spectroscopy and X-ray powder diffraction using pair distribution function analysis, the latter enabling the identification of short-range order in poorly crystalline materials. TiO_2 hydrate was precipitated from HCl in either the anatase or the rutile structure. Unlike from H_2SO_4, the natural structure formed without the use of structure determining agents is rutile. However, seed preparation using 0.4 mol H_3PO_4 per mole of Ti (resulting in 0.35 wt% H_3PO_4 in the hydrate) results in anatase hydrate formation. Sodium citrate or citric acid addition also seed anatase hydrate. The mechanism for polymorph control may be kinetic rather than a structural template or surface adsorption. This process has the potential to be used for the commercial scale production of the TiO_2 pigment. Anatase hydrate has the advantage that traces of iron may be more readily removed by washing than from rutile precipitate, making the HCl process from ilmenite feasible for pigment grade material.

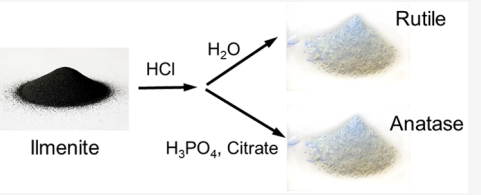

INTRODUCTION

Titanium dioxide is an important pigment used for paints (60% of production), plastics (20%), paper (5%), and other uses (15%) with a world production capacity of 8.4 million tonnes per annum.[1] TiO_2 used for pigments is mostly the rutile phase, which has a higher refractive index and opacity. There is also a small but increasing demand for TiO_2, mostly in the anatase form, for uses including photocatalysts for hydrogen production,[2] dye sensitized photovoltaic cells,[3] photocatalytic degradation of plastics and pollutants,[4,5] electrocatalysts,[6] and anode materials.[7]

The two routes to the commercial production of TiO_2 are known as the sulfate and the chloride routes.[8,9] The older sulfate route normally uses an ilmenite ($FeTiO_3$) feedstock, which is dissolved in sulfuric acid, and from this solution TiO_2 is precipitated. The TiO_2 precipitates as anatase, which is then converted on calcination, with suitable additives, to the thermodynamically and commercially favored rutile. A by-product of the sulfate process is the production of iron sulfate solution which was traditionally dumped at sea but can now be recycled to regenerate H_2SO_4 and iron oxide.

The alternative chloride route, originally developed by Dupont, reacts a high grade rutile ore (which may be natural or synthetic) with Cl_2 to produce $TiCl_4$. This volatile liquid is then hydrolyzed to produce rutile pigment. Earlier, the more abundant Ti containing ore, ilmenite, was not a suitable feedstock, and only rutile ores were suitable, or ilmenite that has been chemically beneficiated to remove most of the iron component. However, the process has been improved to be able to handle Ti ores with a higher Fe content.

A proposed alternative commercial process for the production of TiO_2 directly from ilmenite is the dissolution in hydrochloric acid and precipitation of TiO_2 directly from this Ti and Fe containing solution. This would have several potential advantages. $FeCl_2$ is readily crystallized from the digestion solution and can be roasted to regenerate HCl, providing economic and environmental benefits. Some ilmenite ores are readily soluble in hydrochloric acid without pretreatment,[10,11] enabling a low cost processing stage. Because of the volatility of hydrochloric acid, it is readily removed from the TiO_2 hydrate. Hydrochloric acid is usually coproduced with sodium hydroxide and therefore, depending on the demand for NaOH in, for example, wood pulp leaching, hydrochloric acid may be a relatively low cost reagent.

In the work presented here, the production of TiO_2 hydrate by direct precipitation from hydrochloric acid digestion liquors of ilmenite, with the full Fe content still present in the liquor, is investigated. The formation of rutile or anatase during the precipitation process and factors that control the nucleation and development of different phases is investigated. Control of

Received: February 9, 2022
Revised: April 13, 2022
Accepted: April 18, 2022
Published: April 28, 2022

https://doi.org/10.1021/acs.iecr.2c00463
Ind. Eng. Chem. Res. 2022, 61, 6333−6342

the TiO_2 hydrate phase is attempted with structure determining agents consisting of phosphoric acid or citric acid, and the nature of the seed structure is investigated.

EXPERIMENTAL METHODS

Ilmenite Digestion. Ilmenite concentrate from Barrytown, Westland, New Zealand was supplied by Rio Tinto Pty Ltd. The ilmenite was ground to a 10 μm median particle size. The ground ilmenite was digested in 32% w/w HCl (8.8 mol kg^{-1} HCl or 10.3 M HCl at 20 °C) at a temperature of 85 °C for 3 h. The ratio of acid to ilmenite was 8.50 mol HCl:1 mol $FeTiO_3$ (with the $FeTiO_3$ content of the ore determined by analysis). Digestion of ground ilmenite in hot HCl took place in a 3 L glass flask, fitted with a reflux condenser, and with a Teflon paddle stirrer on a glass shaft. The vessel was placed on a heating element to preheat the HCl before ilmenite addition. Further details of the ilmenite dissolution and kinetics, especially those pertaining to the critical issue of preventing hydrolysis from occurring in the digestion liquor, are detailed elsewhere.[10] Iron filings were added to the liquor sufficient to reduce the small amount of Fe^{3+} to Fe^{2+} and to reduce a small portion (ca. 1%) of the Ti^{4+} to Ti^{3+}. The Ti^{3+} acts as a redox buffer to ensure no Fe^{3+} is present at any time during hydrolysis or filtering. Concentrations of Ti^{4+}, Ti^{3+} and Fe^{2+} were determined by redox titration with a cerium sulfate solution. Ti^{3+} was determined by direct titration to the methyl blue end point, and the total Ti and Fe were determined after reduction with aluminum by titration to methyl blue and N-phenylanthranilic acid end points. The digestion liquor was filtered hot through glass fiber filter paper, Whatman, GFA, and stored at 60 °C, to prevent $FeCl_2$ crystallization, for up to 18 h.

Hydrolysis. Hydrolysis of titanium from the hydrochloric acid solutions containing titanium and iron was performed in a 2 L round bottomed flask, placed in a heating mantle, and stirred by a Teflon paddle (Figure S1, Supporting Information). The hydrolysis procedure was to prepare a "seed" by adding a portion of the liquor (typically 2% of the total liquor to be added) to water at 95−98 °C. The volume of water for the seed to the total liquor volume to be added is here referred to as the "drop ratio" and was typically 20 vol % water to 80 vol % liquor. Therefore, for example, 16 mL of liquor might be added to 200 mL of water, and later 780 mL of liquor would be added (for 2% seed, 80:20 drop ratio). The liquor for seed was added over about 60 s with stirring, with the water held at around 95−98 °C for 5 min to age the seed. Samples of seed were removed and separated by centrifugation for analysis.

After seed aging, the seed solution was brought to a boil, and the remaining hot liquor was added over about 30 min with stirring and sufficient heating to maintain a boil. The slurry containing the hydrate is then aged at a boil for 90 min, before filtering hot. The filter cake was washed immediately with room temperature aqueous 5% HCl.

Structure Determining Agents. The water used for the seed preparation was either deionized water or deionized water with a "structure determining agent" added. The structure determining agent consisted of phosphoric acid or citric acid or citric acid neutralized with NaOH to pH 7.

Elemental Analysis. The elemental composition of the ilmenite and titanium dioxide hydrate were determined by Spectrachem Analytical Services, Lower Hutt, New Zealand. The analyses were performed on a Siemens SRS303AS wavelength dispersive X-ray fluorescence spectrometer. For ilmenite, the samples were prepared by borate fusion. For titanium dioxide hydrates, pressed powder samples were used with the Siemens "Spectraplus" semiquantitative multielement analysis. The relative proportions of FeO and Fe_2O_3 were determined by redox titration of solutions of ilmenite dissolved in acid where air had been excluded.

Structure Determination. The crystal phases in the seed and hydrate were analyzed by Raman spectroscopy and X-ray scattering with pair distribution function (PDF) analysis.[12−14] The hydrate was characterized by X-ray diffraction with Rietveld analysis and X-ray scattering pair distribution function analysis.

Raman Spectroscopy. Continuous wave excitation was used for all Raman measurements. A ThorLabs HeNe laser provided 3−5 mW of 633 nm excitation at the sample. A Modu-Laser Stellar-Pro argon laser provided 6−8 mW of 514.5 and 458 nm excitation at the sample. Raman and Rayleigh scattering light was collected from the sample cell using a 180° backscattering geometry. Rayleigh scattering was rejected using Raman edge filters from Iridian Technologies. The scattered photons were focused onto the entrance slit (100 μm) of an Acton Spectra Pro 2550i 0.500 m imaging single stage monochromator/spectrograph and detected with a Roper Scientific Spec-10:100B CCD detector, controlled by WinSpec software. The detector was liquid nitrogen cooled to −110 °C. Raman scattering was dispersed with a 1200 g/mm holographic diffraction grating.

X-ray Scattering. X-ray scattering patterns were collected on the Powder Diffraction beamline of the Australian Synchrotron which had a Mythen II detector.[13,15,16] For the seed and hydrate, data were recorded at four nominal detector positions for each sample and setup variable. This allowed data to be collected over the angle range 0.2° to 149° in 2θ. Analysis of the data was carried out following merging of these histograms into one pattern with a uniform step size in 2θ (but therefore varying in Q).

An X-ray wavelength, λ, of 0.59074(1) Å (21 keV) was used, which is the maximum operable energy for the monochromator setup available. λ was determined accurately through Rietveld analysis of the diffraction pattern from LaB_6 (NIST standard 660a). A short wavelength, in combination with recording data to a large diffraction angle, 2θ, was necessary to obtain data to high Q space.

Samples were packed in 0.3 mm boron-rich glass capillaries, with a 0.01 mm wall thickness (W. Müller, Schönwalde). Packing densities were measured for all samples and ranged from 25 to 35% based on the expected solid density of crystalline forms of the materials.

In addition to scattering patterns being measured from the samples, data from the empty capillary were recorded, as were data from the vacant beam X-ray path (background). Acquisition times were varied from 10 to 3600 s. Data were normalized to the incoming beam intensity by using the integrated ion chamber counts, divided by the acquisition time. Due to the decaying synchrotron beam, the X-ray intensity variation between electron beam injections was ∼25%.

Data processing to obtain the pair distribution function information used the freely available program PDFGetX2.[17] The observed PDFs were modeled using the program PDFgui,[18] also freely available.

Processing of Total Scattering Data. The X-ray scattering data were first normalized for incoming beam intensity, and then four diffraction patterns were merged to

https://doi.org/10.1021/acs.iecr.2c00463
Ind. Eng. Chem. Res. 2022, 61, 6333−6342

generate one continuous pattern over the angular range under investigation. These data were then processed to subtract the background and are plotted in reciprocal space, Q, where $Q = 4\pi \sin \theta/\lambda$.

The total scattering function, $S(Q)$, which is the normalized total scattering intensity plotted in Q space, was then calculated. While the signal-to-noise ratio looks poor at high Q, the information content is high due partly to the large number of points at which the data are collected. A multipoint moving average could be used to reduce the noise in $S(Q)$. However, such an approach would be merely cosmetic, and there is no advantage to processing the data in this way as the determination of the pair distribution function involves a Fourier transform of these data, effectively dealing with this noise.

The atomic pair distribution function, or the reduced pair distribution function, $G(r)$, which is used here, is the Fourier transform of the total scattering intensity (Figure 2b). This Fourier transform has a fundamental physical significance, which is a representation of the atomic pair density. This relationship allows direct measurement of the relative positions of atoms in a solid[14]

RESULTS

Ilmenite Composition. The ilmenite used contains a slight excess of Ti over Fe compared with the stoichiometry of $FeTiO_3$ (Table 1). Most of the Fe is present as Fe(II), which is relatively unusual, with many resources having higher Fe(III) than in this deposit. There are inclusions of aluminosilicates such as feldspars and phosphates such as apatite and monazite.[19,20]

Table 1. Ilmenite Composition (of Barrytown Concentrate)

oxide	concentation wt % as oxide
TiO_2	47.1
FeO	37.5
Fe_2O_3	3.0
SiO_2	5.2
Al_2O_3	2.3
MnO	1.7
MgO	0.2
CaO	1.1
Na_2O	0.3
K_2O	0.3
P_2O_5	0.2
V_2O_5	0.1
Nb_2O_5	0.05
Ta_2O_5	0.005

Dissolution and Liquor Composition. In order to prevent $FeCl_2 \cdot 4H_2O$ from crystalizing from the digestion liquor, the liquors need to be maintained warm, so they were stored at 60 °C in a water bath between preparation and use for hydrolysis. Degradation of the liquors occurs by the onset of hydrolysis of the titanium component, therefore the liquors were used within 18 h of production. This also necessitated several different batches of liquor to be prepared to complete the hydrolysis trials, each with a slightly differing composition. The range of compositions of the liquors produced are listed in Table 2, with the concentration of the Fe and Ti component represented as the mass of their oxides (as is conventional in the industry).

Table 2. Typical Digestion Liquor Composition Prior to Hydrolysis of the Major Components where M = Mn, Ca, K, Na, Mg

component	equivalent as an oxide	concentration g kg^{-1} (as oxide for Fe and Ti)	concentration, mol kg^{-1}
$FeCl_2$	FeO	85 ± 7	1.18
"$TiOCl_2$"	TiO_2	91 ± 3	1.14
$TiCl_3$	$TiO_{1.5}$	5 ± 3	0.07
HCl	HCl	85 ± 15	2.33
MCl_x	MCl_2	4 ± 2	0.04

Seeding for Analysis and Hydrolysis. Seeding for hydrolysis was performed in situ, with separate seed preparation for analysis of the seed structure. The amount of structure determining additive (phosphate or citrate) used to control the seed formation can be calculated on the basis of the concentration in the aqueous solution or as a proportion of the titanium in the digestion liquor to be added (which is dependent on the level achieved during ilmenite digestion and varies). It can also be represented as a proportion of the amount of total titanium that will be hydrolyzed with this seed, and this latter measure is useful in the case of phosphate, which is nonvolatile and will end up in the precipitated hydrate and in the calcined TiO_2. Phosphate also acts as a structure determining agent in calcination, favoring the formation of anatase.[8] Here, we present the concentrations of additives used for seed formation as moles of structure determining agent to moles of titanium in solution. The phosphate level of 0.4 mol P/mol Ti in the seed solution is equivalent to 0.35% P_2O_5 per mol of Ti when the hydrolysis is completed (based on 2% of the liquor used in the seeding stage).

The seed is a gel-like substance that cannot be separated by filtration but was instead separated by centrifugation after quench cooling.

Hydrolysis. Hydrolysis was carried out via initiation by seed prepared either with just digestion liquor in water or using digestion liquor in water containing phosphoric acid, trisodium citrate, or citric acid (Table 3). There was some variation in the product formed with the same seed type.

For the water-based seed, the hydrate contained 95−100% rutile (by XRD). In addition to the three water seeded hydrate materials presented here, three other water seeded hydrates were produced, not shown, on a larger scale, where two produced 100% rutile and one gave 95% rutile. Therefore, rutile was confirmed to be the consistent product formed with water seeding.

For the phosphate seeded hydrate, the anatase content varied between 100 and 0%. The dominant product from phosphate seed is pure anatase, but the variation experienced here shows that the system is delicate, and some minor factors that were not well controlled can lead to a different product. In addition to the three phosphate seeded hydrate materials presented here, nine other phosphate seeded hydrates were produced, not shown, on a larger scale, where seven produced 100% anatase, one gave 88% anatase, and one was 100% rutile. This suggests that, with experience and careful control, it should be possible to produce exclusively anatase or rutile by this method.

For the citrate seeded hydrate, one citrate and the citric acid based seed resulted in pure anatase, while one other citrate seeded hydrate resulted in a mixed anatase/rutile hydrate.

https://doi.org/10.1021/acs.iecr.2c00463
Ind. Eng. Chem. Res. 2022, 61, 6333−6342

Table 3. Hydrolysis Conditions

label	expt description	additive on the basis of mol P or mol citrate/ mol Ti in seed solution	additive in seed water (P or citrate) mol/kg	drop ratio (by volume) liquor/seed water	% liquor used for seed	liquor Ti (net), g kg^{-1} TiO_2	liquor Fe, g kg^{-1} FeO	anatase/rutile in hydrate by Raman, %:%	anatase/rutile in hydrate by XRD, %:%
HW1	water seeded hydrate 1	0		80:20	2	97	98	rutile (trace anatase)	2:98
HW2	water seeded hydrate 2	0		80:20					0:100
HW3	water seeded hydrate 3	0		80:20	2	78	79	rutile (trace anatase)	0:100
HP1	phosphate seeded hydrate 1	0.4	5.9	80:20	2	90	83	anatase	98:2
HP2	phosphate seeded hydrate 2	0.4	5.9	80:20	2	90	83	rutile and anatase	29:71
HP3	phosphate seeded hydrate 3	0.4	9.7	80:20	2	55	50		100:0
HC1	trisodium citrate seeded hydrate 1	0.4	5.7	80:20	2	93	81		48:52
HC2	trisodium citrate seeded hydrate 2	0.4	5.4	80:20	2	98	79		100:0
HC3	citric acid seeded hydrate 1	0.4		80:20	2				100:0

Yields of 93−96% of the TiO_2 were obtained. Part of the TiO_2 loss is due to the Ti in the form of Ti^{3+} acting as a redox buffer. On a larger scale, less oxidation can occur, so the level of Ti^{3+} could be reduced with a consequently higher yield of Ti during hydrolysis.

Raman of Hydrolysis Product. A reference Raman spectrum of Degussa P25 calcined TiO_2 was recorded (Figure 1a). This material contains a mixture of typically 25% rutile and 75% anatase. Raman shifts characteristic of anatase (393, 513, 636 cm^{-1}) and rutile (438, 607 cm^{-1})[21] are observed in this spectrum with the anatase peaks of higher intensity. These Raman shifts are characteristic of B_{1g}, A_{1g}, and E_g modes for anatase and E_g and A_{1g} modes for rutile, respectively.[22] The B_{1g} peak is caused by the symmetric bending vibration of O−Ti−O. The E_g peak is mainly due to the symmetric stretching vibration of O−Ti−O, and the A_{1g} peak corresponds to the antisymmetric bending vibration of O−Ti−O in TiO_2.

The Raman of the washed and dried (at 110 °C) TiO_2 hydrate (Figure 1a) show peaks characteristic of anatase (393, 513, 636 cm^{-1}) and rutile (438, 607 cm^{-1})[21] in varying proportions for the different hydrates. The peaks are relatively sharp, not too much broader than a sample of Degussa P25 TiO_2 run as a standard, indicating quite good structural homogeneity. The water hydrates 1 and 2 (HW1, HW2) appear to be dominated by rutile with just a hint of anatase, whereas the phosphate hydrate 1 (HP1) is anatase, while phosphate hydrate 2 (HP2) is rutile with some anatase present.

Raman of Seed. The seed material prepared for hydrolysis, or separate seed preparation, which was collected for analysis, is listed in Table S1, Supporting Information. The dried "seed" has broader Raman peaks than for the hydrate (or calcined material) either as a result of the high proportion of atoms at the surface because of the small size or because of other structural disorder.

The seed prepared in water that leads to rutile hydrate has a rutile peak at 438 cm^{-1} and a peak at 613−616 cm^{-1}, which is close to the rutile peak expected at 607 cm^{-1}. Peak broadening and peak shifts in anatase and rutile E_{g1} and A_{1g} modes can result from decreasing crystallite size and structural disorder,[23] and this is the likely explanation for the blue shift in the A_{1g} peak. This seed also shows an anatase peak at 513 cm^{-1}. The Raman indicates, therefore, that the seed is a nanostructured mixed rutile and anatase.

The seed formed from phosphate solution has much broader Raman peaks. The peak for anatase that would be expected at 393 cm^{-1} (as is seen in the hydrate) is shifted to a lower wavenumber in the seed at around 377 cm^{-1}. The peak for anatase expected at 636 cm^{-1} (found in the hydrate) is also not present in this position in the seed but is red-shifted to about 621 cm^{-1}. This is intermediate between the anatase peak and the 607 cm^{-1} peak of rutile. The 607 cm^{-1} peak of rutile and the 636 cm^{-1} peak of anatase are for different vibrational modes. This shift in the anatase peak to 621 cm^{-1} is likely to be due to the decreased crystallite size and structural disorder.[23] There is evidence of a rutile peak at 438 cm^{-1} in this seed, so some rutile is present in the predominantly anatase material.

No peaks characteristic of amorphous titanium phosphates are observed in the seed prepared with phosphate solution. Titanium phosphates have Raman peaks, within the range we studied here, at 411 cm^{-1}, 440 cm^{-1}, 568 cm^{-1}, and 610 cm^{-1} (Ti−O modes) and 532 cm^{-1} (O−P−O bending).[24] We do not see evidence from the Raman spectra of titanium

https://doi.org/10.1021/acs.iecr.2c00463
Ind. Eng. Chem. Res. 2022, 61, 6333−6342

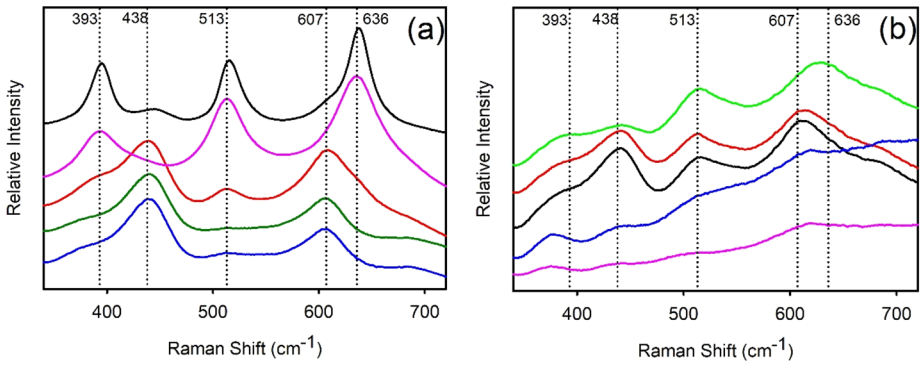

Figure 1. Raman spectra of dried titanium seed and hydrate. (a) Degussa P25 reference (calcined) material, black line; phosphate hydrate 1 (HP1), magenta; phosphate hydrate 2 (HP2), red; water hydrate 1 (HW1), blue; water hydrate 2 (HW2), green. (b) Raman spectra of dried TiO_2 hydrate "seed": water seed 1 (SW1), black; water seed 2 (SW2), red; water seed 3 (SW3), green; phosphate seed 1 (SP1), magenta; phosphate seed 2 (SP2), blue.

phosphate in the seed. Considering that the ratio of P to Ti in the seed solution is 0.4, sufficiently high in phosphorus for it to be a significant component of a precipitate, it would appear that the phosphate remains in solution and does not form a major part of the seed.

The seeds prepared with citric acid and trisodium citrate were not saved for analysis.

XRD and PDF of Hydrolysis Product. The hydrolysis products from TiO_2 seeded with water, phosphate, and citrate all give clearly defined Bragg peaks. The data were collected to high Q enabling analysis of the data both by Rietveld and pair distribution function (PDF) methods. The advantage of applying the PDF method is that this can also be used on very poorly crystalline material where no Bragg peaks are present, such as for some of the seed material. The diffraction spectra for a representative selection of TiO_2 hydrates prepared with seed prepared in water or in phosphate are shown in Figure 2.

To process these same data using PDF requires a series of steps, illustrated in Figure 3. In this method, fitting is done to a structure with the reduced PDF, the $G(r)$, which is a plot of the interatomic distances versus intensity (obtained by Fourier

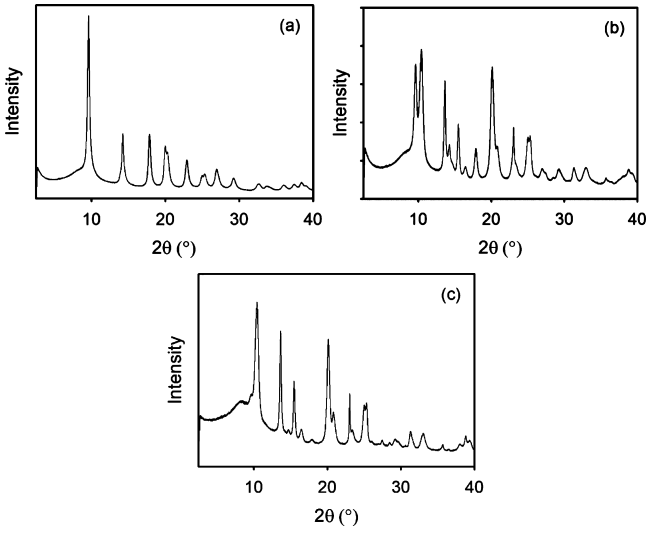

Figure 2. (a) TiO_2 hydrate phosphate seeded 1 (anatase; SP1), (b) TiO_2 hydrate phosphate seeded 2 (mixed anatase/rutile; SP2), (c) TiO_2 hydrate water seeded 1 (rutile; SW1).

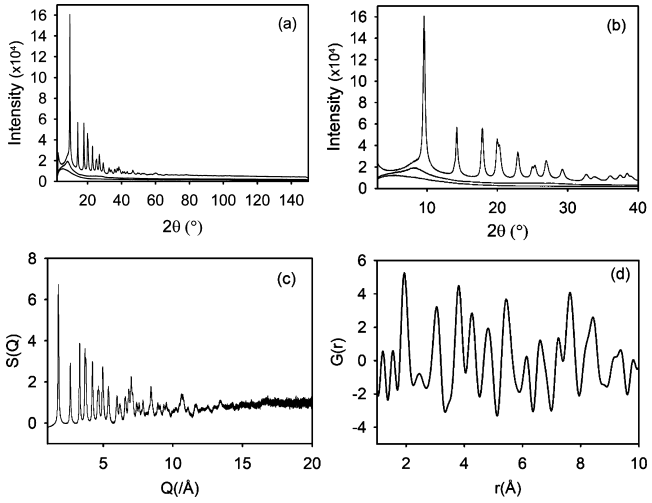

Figure 3. Nanocrystalline TiO_2 hydrate (phosphate seeded hydrate 1). (a,b) Diffraction data in 2θ for 21 keV X-ray energy with air background and capillary scattering (expanded scale for b). (c) Total scattering function, $S(Q)$. (d) Reduced PDF experimental data showing the interatomic spacings.

transform). Therefore, unlike with the diffraction method using Rietveld, short-range order should be all that is needed to achieve this fit provided that there are common bonding lengths.

The reduced PDF can be fitted to known structural data. For the hydrate prepared with phosphate in the seed water and the hydrate prepared from plain seed water, good fits were obtained between the library structures (obtained from the Crystallographic Open Database) and the reduced PDFs (Figure 4). The cell dimensions obtained by allowing an unconstrained fit to these parameters provides a close match to library data for crystalline materials. The crystallite size can also be estimated from the particle diameter obtained from the PDF shape damping function (Table 4).

Pair Distribution Function and Rietveld Analysis of Seed. X-ray scattering analysis of seed material separated by centrifuging (with a translucent gel appearance) some crystallinity for the water based seed (Figure 5a,b) but largely amorphous material for the phosphate based seed (Figure 5b).

A Rietveld analysis of the water based seed gave a structure with the crystalline component at 61% anatase and 39% rutile.

https://doi.org/10.1021/acs.iecr.2c00463
Ind. Eng. Chem. Res. 2022, 61, 6333−6342

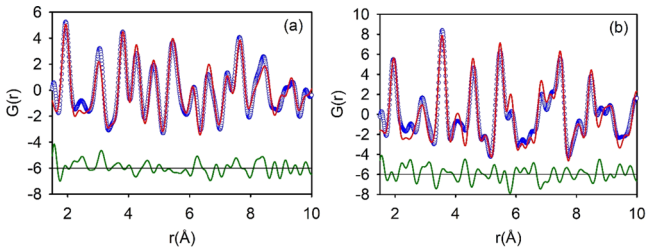

Figure 4. Reduced PDF (blue circles) with the fitted structure (red line) and residuals (green line): (a) anatase hydrate 1; (b) rutile hydrate 1.

Interestingly, this mixed seed leads to an almost pure rutile hydrate.

Crystal structures for anatase or rutile were not able to be fitted to the pair distribution function of the X-ray data for the phosphate seed. The PDF from this seed material does show what appears to be some structure with structured peaks in the plot up to about 3.5 Å. This suggests just short-range order in the material. However, there is a very low intensity for $G(r)$ (Figure 5c) so that caution must be applied in interpreting these data.

The experimental PDF for the seed is then compared with the modeled PDF for anatase and rutile with crystallographic parameters adjusted to fit to the respective hydrates (Figure 5d). From this comparison, the atom pair spacing peaks in SP2 at ca. 2 Å (Ti−O) could be for either anatase or rutile and with maybe a second peak above 3 Å (Ti−Ti), which coincided more closely with anatase[25,26] but not unequivocally because the important longer range order peaks are not well defined. This gives some measure of the lack of long-range order in the material.

Elemental Analysis of Hydrolysis Product. The elemental composition of the hydrolysis product for both the phosphate seeded hydrate and the water seeded hydrate is similar, except for the increased phosphate content of the phosphate seeded material. The difference in phosphate content is similar to the amount of phosphate added, indicating that it is quantitatively deposited in the hydrate (as is the phosphate originally present in the ilmenite). Tantalum and niobium are also quantitatively precipitated with the TiO_2. The elements Si, Al, Ca, and K are also present, but at low levels compared with the amount present in the ilmenite. We have not investigated how these are incorporated into the hydrate, whether as small undissolved gangue particles or as chemically precipitated components. Nevertheless, the elements Si, Al, Ca, and K do not normally produce highly colored materials, and these elements normally form a major part of the coatings typically applied to pigment grade TiO_2, so at these levels they are not detrimental.

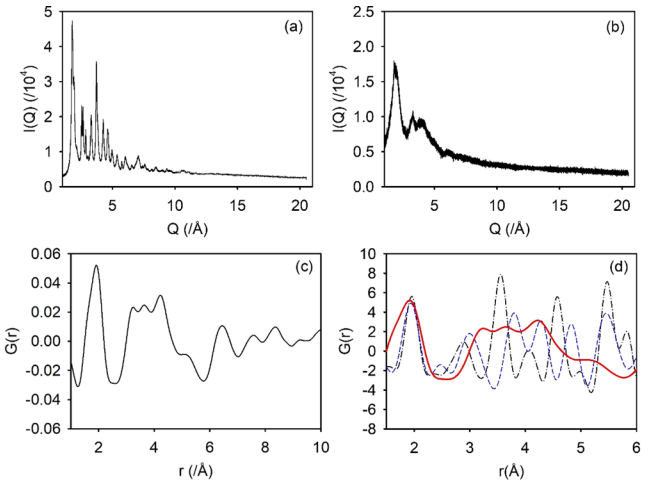

Figure 5. X-ray scattering intensity (IQ) for (a) seed SW3 after subtraction of the background for the capillary in air; (b) seed SP2 (seed SP1 looks similar—not shown); (c) seed SP2 G9(r); (d) seed SP2 G(r) scaled × 100 (red solid line) compared with anatase (blue dashed line) and rutile (black dot dash line) from the fitted form for the hydrates.

Iron Content. Although the values in Table 5 show higher iron contents, with careful washing of large samples where a thick filter cake was formed, it was possible to get the anatase hydrate iron content in the range 8−20 ppm, whereas for the rutile hydrate only 100−300 ppm could be achieved (0.01−0.03% Fe). It is not clear why there was this difference between anatase and rutile, but this difference is large in the context of pigment quality. One explanation could be that because the anatase hydrate made a more easily washable filter cake with

Table 5. Hydrate Composition (Typical Analyses)

oxide	anatase (phosphate seeded), wt %	rutile (no structure determining agent), wt %
TiO_2	94.3	95.8
P_2O_5	0.82	0.49
Nb_2O_5	0.13	0.13
Ta_2O_5	0.009	0.009
Cl	4.4	3.1
FeO	0.015 (120 ppm Fe)	0.044 (340 ppm Fe)
SiO_2	0.19	0.28
Al_2O_3	0.07	0.03
CaO	0.01	0.02
K_2O	0.006	0.01

Table 4. PDF and Rietveld Analysis of Two Representative Titanium Oxide Hydrates, with Two Library Crystal Structures for Comparison

sample	% anatase from XRD Rietveld	% rutile from XRD Rietveld	cell dimension a and b, Å	cell dimension c, Å	crystallite size, Å
anatase hydrate (phosphate seeded 1) PDF			3.7830	9.5055	21
anatase hydrate (phosphate seeded 1) Rietveld	98	2	3.7813	9.4780	22
CIF 9008213 anatase[27]	100		3.7842	9.5146	
rutile hydrate (water seeded 1) PDF			4.6051	2.9602	45
rutile hydrate (water seeded 1) Rietveld	2	98	4.5872	2.9443	670
CIF 9001681 rutile[28]		100	4.5922	2.9574	

https://doi.org/10.1021/acs.iecr.2c00463
Ind. Eng. Chem. Res. 2022, 61, 6333−6342

fast flow rates compared with the rutile hydrate, then better and more uniform washing was achieved with the anatase hydrate. Another possible explanation may be that there is stronger surface adsorption (or internal absorption) of iron on the rutile hydrate. We have not been able to determine the cause of this difference in iron content, but it is an important consideration for the commercial production of titanium dioxide.

Calcination of Hydrate to Produce Pigment. Calcination of the titanium dioxide hydrate is required to form pigment material with suitable qualities, such as particle size, crystal phase, and color. The favored polymorph of TiO_2 for most commercial applications is rutile. Rutile is the thermodynamically favored form (lowest energy). Calcination from rutile structured hydrate to rutile TiO_2 requires careful control to achieve a suitable particle size, aspect ratio, and other properties. Calcination from anatase structured hydrate in addition requires the conversion to rutile. A study of these processes is beyond the focus and scope of this manuscript and will be published separately. However, two points can be noted. Additives are typically added to assist (or hinder) the conversion of anatase to rutile in commercially produced material from the sulfate process (that produces an anatase hydrate) and to control the texture of the pigment produced from any hydrate.[29] Phosphate is known to hinder the conversion of anatase to rutile. With the titanium dioxide hydrates produced here from HCl digestion of ilmenite, it was possible on calcination to produce a rutile pigment, even with the level of phosphate added for anatase seeding and the phosphate present from the ore. A UV/vis spectrum of these calcined materials is available in Supporting Information Figure S2.

DISCUSSION

Ilmenite Source and Suitability. Whereas most modern industrial methods to produce TiO_2 pigment first require ores to be upgraded to a high rutile content, it is possible to dissolve New Zealand ilmenite directly in hydrochloric acid[10] without pretreatment to get a solution with a high concentration of Ti^{4+}. This deposit contains over 12 M tonnes of ilmenite at a 2% cutoff grade,[30] with other similar size deposits nearby. The ilmenite digestion solution in HCl is suitable for hydrolysis to form titanium dioxide hydrate that can be calcined to pigment grade material. It has the advantage of low levels of V and Cr, which, when present in ilmenite, can produce highly colored compounds adversely affecting pigment quality. Other ilmenite sources were not investigated for HCl solubility in this work, other than a brief investigation of Minnesota ilmenite (data not presented here), which was found to be very soluble in HCl but contains higher levels of V. In general, the solubility of ilmenite in HCl may be different from the solubility in H_2SO_4 and is dependent on a number of factors including the relative proportions of Fe(II) and Fe(III) in the ore and the nature of inclusions.

HCl Hydrate Is Rutile. The digestion liquor obtained from hydrochloric acid dissolution of New Zealand ilmenite results naturally in a rutile structured hydrate when seeded with liquor and water seed without added phosphoric of citric acid (Table 3). This is in contrast to the industrial sulfate process, a similar solution-based hydrolysis but from sulfuric acid, where the naturally formed hydrate is anatase. Sulfate is believed to inhibit the anatase to rutile transformation of hydrate on calcination,[9] and clearly it also controls the precipitation of the hydrate as anatase, unlike hydrochloric acid.

Controlling the Structure of the Hydrate. Here, we show that phosphate can influence the structure of the titanium dioxide formed. Phosphoric acid at a level that amounts to 0.35% P_2O_5 in the final pigment, which was a concentration in the seed water of 5.4−9.7 mol kg^{-1} H_3PO_4 or a molar ratio of P to Ti in the seed of 0.4 results in anatase TiO_2 hydrate forming from hydrochloric acid solution rather than rutile, which forms in the absence of phosphate (Table 3). Phosphate has previously been shown to effect anatase precipitation from $Ti[OCH(CH_3)_2]_4$ solutions[31] and is also know to inhibit conversion of anatase to rutile during calcination.[9,31,32] This has been suggested as being due to surface adsorption of PO_4^{3-} species[31] (and perhaps also SO_4^{2-} species for the sulfate process). However, another possibility might be that the effect of the phosphate is due to the pH buffer effect rather than a surface structural effect.

Therefore citric acid and trisodium citrate were investigated as a means to control the polymorph of TiO_2 that forms from HCl solution where it would act as a pH buffer but perhaps not as a surface structural agent. At a concentration in the seed water of 5.4−5.7 mol kg^{-1} citrate or a molar ratio of citrate to Ti in the seed of 0.4, it was shown here that citrate can also result in an anatase hydrate (Table 3), rather than the rutile hydrate formed in the absence of this addition. Therefore, perhaps controlling the pH is all that is required to control the anatase or rutile formation, although citric acid also forms a polyvalent anion and has the possibility to surface adsorb too.

Variability. However, the variation experienced in the amount of anatase formed with this seeding procedure shows that the system is delicate and some minor factors that were not well controlled can lead to a product containing rutile or exclusively of rutile. Here, we have not determined the precise nature of these factors, but this would be a consideration if this process were to be scaled up. Possible factors include mixing during liquor addition, temperature control, cleanliness of the liquor (lack of fine gangue), storage time and temperature of the liquor prior to addition, temperature of the surface of the reaction vessel during seeding and hydrolysis, and cleanliness of the reaction vessel prior to the seeding and hydrolysis.

How Does the Seeding Work. To get some understanding of how the phosphate structure determining agent works, the largely amorphous seed material was separated and investigated. For the seed prepared with just water, which leads to rutile hydrate, the seed appears from Raman to be a mixed phase of anatase and rutile (Figure 1b). The shift observed in the peak positions of seed compared with highly crystalline material indicates that the seed has a small crystallite size and some disorder, as would be expected. The seed prepared from the phosphate-containing solution results in a seed that is mainly anatase, again with small crystallites and disorder (Figure 1b). It is not a titanium phosphate material. The phosphate has therefore probably largely remained in solution (later it gets incorporated into the hydrate). X-ray scattering of the phosphate prepared seed material showed that it had only short-range order and that it is more likely to be similar to anatase but that rutile cannot be ruled out (Table S1, Supporting Information).

Because the phosphate does not appear to become part of the seed, we considered how the phosphate might act to control seed formation if it is not acting as a structural template. A pH buffer is one possibility, so an alternative

https://doi.org/10.1021/acs.iecr.2c00463
Ind. Eng. Chem. Res. 2022, 61, 6333−6342

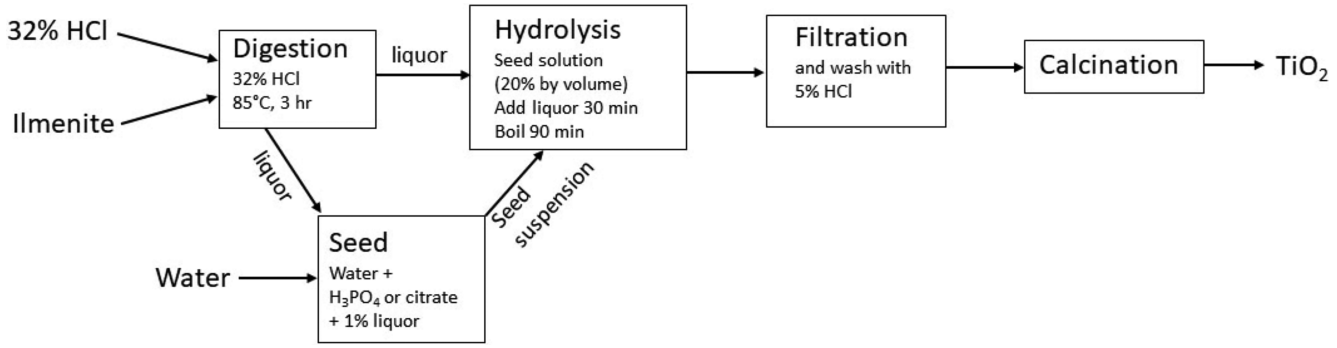

Figure 6. Block process flow diagram for preparation of TiO_2 from ilmenite.

system was tried with citric acid and trisodium citrate. Phosphoric acid has pK_a's of 2.2, 7.2, and 12.4, while citric acid is also triprotic with three pK_a's of 3.1, 4.7, and 6.4. Both of these acids are therefore capable of a broad range of pH buffering.

Buffering of the water used to initiate hydrolysis maintains the solution at a higher pH, which should result in more rapid hydrolysis. A rapid hydrolysis could enable a kinetically favored product to form over a thermodynamically most favored form. Rutile is the thermodynamically favored form. It has been noted in gas phase hydrolysis of $TiCl_4$ that a high temperature with fast reaction favors anatase formation while a lower temperature, slower reaction favors rutile.[9] A similar kinetically favored product appears to be produced here in buffered solution maintaining a higher pH for more rapid hydrolysis to anatase. Both phosphate and citrate enable this, and other suitable buffers should also probably achieve this outcome. However, it should be noted that phosphate, in sufficiently high concentrations, has been shown to affect the conversion of anatase to rutile during calcination[33−35] so that some level of control by phosphate of the seeding of anatase other than as a pH buffer cannot be ruled out from this work. From sulfuric acid, the hydrolysis product is anatase,[32] and it has also been shown that from chloride solutions the addition of sulfate will lead to anatase rather than rutile.[36] While technically the method has now been established with this work, there are still some unanswered scientific questions around the mechanism.

The seed structure leads to the hydrate structure, with the mixed anatase−rutile seed resulting in rutile hydrate and the anatase seed resulting in anatase hydrate (Table 3). However, the buffer capacity of the phosphate or citrate modified added water for hydrolysis may continue to contribute to kinetic control of the hydrate even after the "seed" is formed, so that seeding may be only part of the process of controlling the polymorph of the hydrate with the buffering continuing to control this during the early part of the "drop".

Citrate has an advantage over phosphate in that it will burn off during calcination and is therefore less likely than phosphate to influence the calcination process where development of the required structure of the final pigment occurs.

The overall process is illustrated in Figure 6.

Ilmenite Minor Elements. The source of ilmenite may have an effect on hydrolysis or calcination. Where the ilmenite contains high levels of soluble components that may influence the structure of the hydrolysis product or the conversion of this product during calcination, then the process may need to be adapted to suit the mineral source. New Zealand ilmenite contains inclusions of apatite and monazite,[19] both of which are hydrochloric acid soluble phosphate-containing minerals, but at sufficiently low levels not to limit the options available to control the hydrolysis to anatase or rutile or the conversion of anatase to rutile on calcination. Another deposit containing higher levels of phosphate may result in different behavior. Other elements, such as niobium, can also influence anatase to rutile conversion and crystallite size.[8,9,29,32,37]

Why Anatase Hydrate from HCl Might Be Desirable. Rutile is the desirable form of titanium dioxide for most pigment applications (the main commercial demand for TiO_2). The pigment must also be very white. A white pigment necessitates, among other factors, a low level of colored impurities, of which the main component is typically iron, but sometimes small amounts of transition metals such as V, Cr, or Cu can be troublesome.[9] Here, it was found that it is difficult to obtain a hydrate with a sufficiently low iron content from a hydrate that is rutile. However, because it is possible to control the hydrolysis to form anatase, and the iron washes out of the anatase readily to achieve low levels of iron, it is possible to achieve TiO_2 of sufficient quality for this process to have potential for commercial pigment grade material. To achieve these low levels of iron in the pigment, it is not necessary to remove the iron chloride from solution prior to hydrolysis as the iron washes out easily from the anatase hydrate. It is possible that the extra iron in solution assists in stabilizing the titanium in solution and the formation of a suitable hydrate structure. We have been careful to ensure that Fe^{3+} is not present, rather only Fe^{2+}, during the hydrolysis and hydrate washing stage, to avoid the risk of less soluble iron structures forming, although we did not explicitly test this hypothesis in this work.

■ CONCLUSIONS

Hydrolysis of titanium oxide hydrate from solutions of ilmenite dissolved in hydrochloric acid was achieved with controllable formation of anatase or rutile. Rutile was formed when hydrolysis was seeded with digestion liquor in water, but anatase was formed when phosphoric acid, citric acid, or sodium citrate was used in the seed water. The mechanism for polymorph control may be predominantly kinetic, based on pH controlling the rate of hydrolysis. However, surface adsorption of polyvalent anions controlling the structure has not been ruled out. Despite the high iron content of the dissolution liquor, it was possible to wash out the iron from the resulting titanium dioxide hydrate to acceptable levels for pigment production when the hydrate is in the form of anatase, but not when it is rutile. The reason the rutile hydrate retains more iron was not fully investigated but may be due to the

https://doi.org/10.1021/acs.iecr.2c00463
Ind. Eng. Chem. Res. 2022, 61, 6333−6342

better filtration characteristics of the anatase hydrate. This process has the potential to be used for the commercial scale production of the TiO_2 pigment.

■ ASSOCIATED CONTENT

Supporting Information

The Supporting Information is available free of charge at https://pubs.acs.org/doi/10.1021/acs.iecr.2c00463.

Figure for hydrolysis experimental arrangement; table of seed preparation for Raman and X-ray analysis of seed; method and figure for UV/vis spectra (PDF)

■ AUTHOR INFORMATION

Corresponding Author

Richard G. Haverkamp − *School of Engineering and Advanced Technology, Massey University, Palmerston North 4472, New Zealand;* orcid.org/0000-0002-3890-7105; Email: r.haverkamp@massey.ac.nz

Authors

Kia S. Wallwork − *NST Central, ANSTO, Lucas Heights, New South Wales 2234, Australia*

Mark R. Waterland − *Institute of Fundamental Sciences, Massey University, Palmerston North 4472, New Zealand;* orcid.org/0000-0002-8493-9407

Qinfen Gu − *Australian Synchrotron, ANSTO, Clayton, Victoria 3168, Australia;* orcid.org/0000-0001-9209-4208

Justin A. Kimpton − *Australian Synchrotron, ANSTO, Clayton, Victoria 3168, Australia*

Complete contact information is available at: https://pubs.acs.org/10.1021/acs.iecr.2c00463

Notes

The authors declare no competing financial interest.

■ ACKNOWLEDGMENTS

This research was undertaken on the PD beamline at the Australian Synchrotron, part of ANSTO. The New Zealand Synchrotron Group provided travel and accommodation.

■ REFERENCES

(1) Gambogi, J. *Titanium and Titanium Dioxide. Mineral Commodity Summaries*; U.S. Geological Survey: Reston, VA, 2021.

(2) Ismael, M. Latest progress on the key operating parameters affecting the photocatalytic activity of TiO2-based photocatalysts for hydrogen fuel production: A comprehensive review. *Fuel* **2021**, *303*, 121207.

(3) Saeed, M. A.; Yoo, K.; Kang, H. C.; Shim, J. W.; Lee, J. J. Recent developments in dye-sensitized photovoltaic cells under ambient illumination. *Dyes Pigm.* **2021**, *194*, 109626.

(4) Nabi, I.; Bacha, A. U. R.; Ahmad, F.; Zhang, L. Application of titanium dioxide for the photocatalytic degradation of macro- and micro-plastics: A review. *J. Environ. Chem.Eng.* **2021**, *9*, 105964.

(5) Das, A.; Adak, M. K.; Mahata, N.; Biswas, B. Wastewater treatment with the advent of TiO_2 endowed photocatalysts and their reaction kinetics with scavenger effect. *J. Mol. Liq.* **2021**, *338*, 116479.

(6) Lavacchi, A.; Bellini, M.; Berretti, E.; Chen, Y.; Marchionni, A.; Miller, H. A.; Vizza, F. Titanium dioxide nanomaterials in electrocatalysis for energy. *Curr. Opin. Electrochem.* **2021**, *28*, 100720.

(7) Peng, P. P.; Wu, Y. R.; Li, X. Z.; Zhang, J. H.; Li, Y. W.; Cui, P.; Yi, T. F. Toward superior lithium/sodium storage performance: design and construction of novel TiO2-based anode materials. *Rare Met.* **2021**, *40* (11), 3049−3075.

(8) Buxbaum, G.; Pfaff, G. *Industrial Inorganic Pigments: Third Edition*; Wiley-VCH Verlag GmbH: Weinheim, 2005. DOI: 10.1002/3527603735.

(9) Barksdale, J. *Titanium. Its occurance, chemistry and technology*; The Ronald Press Company: New York, 1966.

(10) Haverkamp, R. G.; Kruger, D.; Rajashekar, R. The digestion of New Zealand ilmenite by hydrochloric acid. *Hydrometallurgy* **2016**, *163*, 198−203.

(11) Olanipekun, E. A kinetic study of the leaching of a Nigerian ilmenite ore by hydrochloric acid. *Hydrometallurgy* **1999**, *53*, 1−10.

(12) Petkov, V. Nanostructure by high energy X-ray diffraction. *Mater. Today* **2008**, *11* (11), 28−38.

(13) Haverkamp, R. G.; Wallwork, K. S. X-ray Pair Distribution Function Analysis of Nanostructured Materials using a Mythen Detector. *J. Synchrotron Radiat.* **2009**, *16* (6), 849−856.

(14) Egami, T.; Billinge, S. J. L. *Underneath the Bragg Peaks: Structural Analysis of Complex Materials*; Permagon: Oxford, 2003.

(15) Schmitt, B.; Brönnimann, C.; Eikenberry, E. F.; Gozzo, F.; Hörmann, C.; Horisberger, R.; Patterson, B. Mythen detector system. *Nucl. Instrum. Meth. A* **2003**, *501*, 267−272.

(16) Wallwork, K. S.; Kennedy, B. J.; Wang, D. The high resolution powder diffraction beamline for the Australian Synchrotron. In *AIP Conf. Proc.*, Wallwork, K. S., Kennedy, B. J., Wang, D., Eds.; AIP: 2007; Vol. *879*, pp 879-882.

(17) Qiu, X.; Thompson, J. W.; Billinge, S. J. L. PDFgetX2: a GUI-driven program to obtain the pair distribution function from X-ray powder diffraction data. *J. Appl. Crystallogr.* **204**, **2004**37 (4), 678.

(18) Farrow, C. L.; Juhas, P.; Liu, J. W.; Bryndin, D.; Bozin, E. S.; Bloch, J.; Proffen, T.; Billinge, S. L. J. PDFfit2 and PDFgui: computer programs for studying nanostructures in crystals. *J. Phys-Condens. Mat* **2007**, *19*, 335219.

(19) Wells, H. C.; Haverkamp, R. G. Characterization of the heavy mineral suite in a holocene beach placer, Barrytown, New Zealand. *Minerals* **2020**, *10* (2), 86.

(20) Duncan, J. F.; Metson, J. B. Acid attack on New-Zealand ilmenite. 2. The structure and composition of the solid. *N.Z. J. Sci.* **1982**, *25* (2), 111−116.

(21) Lafuente, B.; Downs, R. T.; Yang, H.; Stone, N. The power of databases: The RRUFF project. In *Highlights in Mineralogical Crystallography*; De Gruyter: Berlin, 2016; pp 1−29.

(22) Challagulla, S.; Tarafder, K.; Ganesan, R.; Roy, S. Structure sensitive photocatalytic reduction of nitroarenes over TiO2. *Sci. Rep.* **2017**, *7* (1), 1−11.

(23) Swamy, V. Size-dependent modifications of the first-order Raman spectra of nanostructured rutile TiO2. *Phys. Rev. B* **2008**, *77* (19), 1−4.

(24) Schmutz, C.; Barboux, P.; Ribot, F.; Taulelle, F.; Verdaguer, M.; Fernandezlorenzo, C. EXAFS, Raman and P-31 NMR-study of amorphous titanium phosphates. *J. Non-Cryst. Solids* **1994**, *170* (3), 250−262.

(25) Nguyen-Phan, T. D.; Liu, Z.; Luo, S.; Gamalski, A. D.; Vovchok, D.; Xu, W.; Stach, E. A.; Polyansky, D. E.; Fujita, E.; Rodriguez, J. A.; et al. Unraveling the Hydrogenation of TiO2 and Graphene Oxide/TiO2 Composites in Real Time by in Situ Synchrotron X-ray Powder Diffraction and Pair Distribution Function Analysis. *J. Phys. Chem. C* **2016**, *120* (6), 3472−3482.

(26) Fernandez-Garcia, M.; Belver, C.; Hanson, J. C.; Wang, X.; Rodriguez, J. A. Anatase-TiO_2 nanomaterials: Analysis of key parameters controlling crystallization. *J. Am. Chem. Soc.* **2007**, *129* (44), 13604−13612.

(27) Horn, M.; Schwerdtfeger, C. F.; Meagher, E. P. Refinement of the structure of anatase at several temperatures. *Z. Kristallogr. NCS* **1972**, *136* (3−4), 273−281.

(28) Swope, R. J.; Smyth, J. R.; Larson, A. C. H in rutile-type compounds: I. Single-crystal neutron and X-ray diffraction study of H in rutile. *Am. Mineral.* **1995**, *80* (5−6), 448−453.

(29) Hanaor, D. A. H.; Sorrell, C. C. Review of the anatase to rutile phase transformation. *J. Mater. Sci.* **2011**, *46* (4), 855−874.

(30) Caffyn, P. H. *Ilmenite Reserves at Barrytown, New Zealand*; Ministry of Economic Development: Wellington, New Zealand, 1976.
(31) Ohtsuka, Y.; Fujiki, Y.; Suzuki, Y. Impurity effects on anatase-rutile transformation. *J. Mineral. Petrol. Sci.* **1982**, *77*, 117−124.
(32) Karvinen, S. The effects of trace elements on the crystal properties of TiO2. *Solid State Sci.* **2003**, *5* (5), 811−819.
(33) Grzmil, B.; Rabe, M.; Kic, B.; Lubkowski, K. Influence of phosphate, potassium, lithium, and aluminium on the anatase - Rutile phase transformation. *Ind. Eng. Chem. Res.* **2007**, *46* (4), 1018−1024.
(34) Roy, B.; Fuierer, P. A. Influence of sodium chloride and dibasic sodium phosphate salt matrices on the anatase-rutile phase transformation and particle size of titanium dioxide powder. *J. Am. Ceram, Soc.* **2010**, *93* (2), 436−444.
(35) Gesenhues, U. Calcination of metatitanic acid to titanium dioxide white pigments. *Chem. Eng. Technol.* **2001**, *24* (7), 685−694.
(36) Li, Y.; Yang, Y.; Guo, M.; Zhang, M. Influence of acid type and concentration on the synthesis of nanostructured titanium dioxide photocatalysts from titanium-bearing electric arc furnace molten slag. *RSC Adv.* **2015**, *5* (18), 13478−13487.
(37) Arbiol, J.; Cerda, J.; Dezanneau, G.; Cirera, A.; Peiro, F.; Cornet, A.; Morante, J. R. Effects of Nb doping on the TiO_2 anatase-to-rutile phase transition. *J. Appl. Phys.* **2002**, *92* (2), 853−861.

https://doi.org/10.1021/acs.iecr.2c00463
Ind. Eng. Chem. Res. 2022, 61, 6333−6342